Deep convection lifecycle characteristics: a database from GoAmazon experiment

Camila da Cunha Lopes¹, Rachel Ifanger Albrecht¹, Douglas Messias Uba², Thiago Souza Biscaro², and Ivan Saraiva³

Correspondence: Camila da Cunha Lopes (camilalopes.ccl@gmail.com)

Abstract. The Observations and Modeling of the Green Ocean Amazon (GoAmazon2014/5) Experiment provided a comprehensive suite of cloud-aerosol-precipitation observations with both *in situ* and remote sensing instruments. In this study, we apply a tracking methodology to volumetric radar data, creating a refined database focused on deep convective systems with full lifecycle, incorporating lightning data. This refined deep convection database is shown to be a robust sample of the complete dataset in terms of convective systems morphology. The analysis reveals significant seasonal and diurnal variations in convective morphology and intensity, with most intense systems occurring during the dry-to-wet season transition. The filtered dataset offers a robust sample for future studies on Amazonian convection.

1 Introduction

15

The Amazon tropical rainforest serves as a natural test bed for several studies on cloud-aerosol-precipitation and land-atmosphere interactions due to its large territorial extent which includes pristine forest, agricultural expansion and a large urban zone with an industrial center. This complex ecosystem is one of the main centers of convection regulating the climate (Nobre et al., 2009; Artaxo et al., 2022) and the South American Monsoon System (SAMS) (Zhou and Lau, 1998; Jones and Carvalho, 2002). Several convection patterns are present in the region, mainly modulated by the Hadley circulation and the corresponding position of the Intertropical Convergence Zone (ITCZ) which determines the wet (austral summer) and dry (austral winter) seasons.

Several field experiments were conducted in the region in order to study different aspects of the cloud-aerosol-precipitation interactions: the Amazon the Amazon. The Amazon Boundary Layer Experiment ABLE 2A (Harriss et al., 1988) and 2B (Harriss et al., 1990)) focused on the chemistry and dynamics of lower atmosphere in the dry and wet seasons, respectively; the . The Large-Scale Biosphere-Atmosphere Experiment in Amazonia LBA Program (Silva Dias et al., 2002) were responsible for numerous field experiments during late 1990s and early 2000s, including the first major mesoscale atmospheric campaign as part of the Tropical Rainfall Measuring Mission (TRMM) validation campaigns and the CHUVA Project (Cloud Processes of the Main Precipitation Systems in Brazil: A Contribution to Cloud-Resolving Modeling and to the Global Precipitation

¹Departamento de Ciências Atmosféricas, Instituto de Astronomia, Geofísica e Ciências Atmosféricas, Universidade de São Paulo, Rua do Matão, 1226, 05508-090, São Paulo, SP, Brasil

²Divisão de Satélites e Sensores Meteorológicos, Coordenação-Geral de Ciências da Terra, Instituto Nacional de Pesquisas Espaciais, Rodovia Presidente Dutra, Km 40, SP-RJ, 12630-000, Cachoeira Paulista, SP, Brasil

³Centro Gestor e Operacional do Sistema de Proteção da Amazônia, Av. do Turismo, 1350, 69049-630, Manaus, AM, Brasil

Measurement (GPM) (Machado et al., 2014a). The Green Ocean Amazon Experiment (GoAmazon 2014/5) (Martin et al., 2017) was the first long-term experiment to analyze the effects of the Manaus pollution plume in different experimental sites around Manaus, and included two intensive operation periods (IOPs) in the wet and dry seasons. Unlike previous experiments, an operational weather radar was available during GoAmazon, operated by *Sistema de Proteção da Amazônia* (SIPAM, System for the Protection of the Amazon), which covers all experimental sites with cloud remote sensing data in great temporal and spatial resolutions. The main goal of the GoAmazon experiment was to analyze cloud-aerosol-precipitation interactions between the forest and the Manaus metropolitan region, specially the transformation of air plumes from the pristine forest to the Manaus pollution plumes and its eastern propagation. The goal of the CHUVA-Manaus experiment was to characterize the convection regimes in the region by remote sensing, with the installation of a X-Band radar during the experiment and partnerships with CENSIPAM (*Centro Gestor e Operacional do Sistema de Proteção da Amazônia*, Manager and Operational Center of the System for the Protection of the Amazon) for surface radar data and NASA-JAXA (National Aeronautics and Space Administration — Japan Aerospace Exploration Agency) for satellite radar data from TRMM (Tropical Rainfall Measuring Mission) and GPM (Global Precipitation Measurement Mission).

A few studies provide insights about convection characteristics during GoAmazon, such as Giangrande et al. (2017), Machado et al. (2018), Giangrande et al. (2020), and Biscaro et al. (2021). Each of them uses different definitions of cloud features using different sources of remote sensing data and even diverges in the definition of wet and dry seasons, which makes it difficult for other studies to follow a homogeneous methodology of convection measurements, specially the ones that analyze cloud-aerosol-precipitation interactions. For this reason, this study aims to create a comprehensive database and methodology of convective systems based on radar data that can be used in future studies regarding GoAmazon data.

2 Materials and Methods

2.1 Data

35

40

Data sources for this study are the field experiments GoAmazon (Martin et al., 2017) and CHUVA-Manaus (Machado et al., 2014b) that occurred between January 2014 and December 2015 around Manaus, Amazonas. The main goal of the GoAmazon experiment was to analyze cloud-aerosol-precipitation interactions between the forest and the Manaus metropolitan region, specially the transformation of air plumes from the pristine forest to the Manaus pollution plumes and its eastern propagation. The goal of the CHUVA-Manaus experiment was to characterize the convection regimes in the region by remote sensing, with the installation of a X-Band radar during the experiment and partnerships with CENSIPAM (Centro Gestor e Operacional do Sistema de Proteção da Amazônia, Manager and Operational Center of the System for the Protection of the Amazon) for surface radar data and NASA-JAXA (National Aeronautics and Space Administration — Japan Aerospace Exploration Agency) for satellite radar data from TRMM (Tropical Rainfall Measuring Mission) and GPM (Global Precipitation Measurement Mission).

The main site of these experiments, named T3, was located in Manacapuru, Amazonas, Brazil (3.213°S, 60.598°W), about 70 km west from Manaus. A wide range of cloud, precipitation, aerosols and atmospheric instruments were installed at the

site, such as part of the ARM (Atmospheric Radiation Measurement) mobile facility AMF1 that took measurements during the most part of the experiment. Some additional instrument and site (shown in Fig. 1 of Martin et al. (2017)) took measurements during two intensive operation periods (IOPs), with IOP1 being between February 1st and March 31st 2014 (wet season) and IOP2 between August 15th and October 15th 2014 (dry season). More details about the campaigns can be found in Martin et al. (2016, 2017).

In order to create the convective systems database, radar volumes from SIPAM (*Sistema de Proteção da Amazônia*, System for the Protection of the Amazon) single polarization S-band radar located in Manaus (3.149°S, 59.991°W, 102.4 m altitude, Fig. 1) were selected in the period of GoAmazon experiment (2014-01-01 to 2015-12-31). These volumes consist of CAPPIs (Constant Altitude Plan Position Indicators) with a bias correction calculated by Schumacher and Funk (2018). Table 1 shows the data settings, including the bias values applied throughout the period.

This radar has a beamwidth of 1.8° and performs volumetric scans approximately every 12 minutes, covering a domain of 240 km from the radar location with a gate resolution of 500 m, azimuth resolution of 1°, and 17 elevation angles (0.9–19.5°). Given the coarse characteristics of this radar and its scan strategy, such as varying numbers of elevation sweeps and antenna vibrations between volumes, the radar data used in this study consist of quality-controlled, bias-corrected CAPPIs, gridded onto a 1 × 1 km horizontal resolution, following previous studies using the same sourcer of data (e.g., Gupta et al. (2024)). Following the approach of Saraiva et al. (2016), who limited the domain to 150 km radius to ensure better beam geometry and vertical resolution, we also we restricted our analysis to a 150 × 150 km box centered on the radar location. This domain allows for consistent and reliable detection of convective structures while minimizing the effects of beam broadening, ground clutter, and incomplete vertical sampling at farther ranges.

A second data source was employed to calculate parameters related to lightning activity in the convective systems. The Vaisala GLD360 lightning network (Demetriades et al., 2010) measures cloud-to-ground return strokes in the VLF (Very Low Frequency) range using two location triangulation techniques, magnetic direction finding (MDF) and time-of-arrival (TOA), as well as lightning recognition algorithms. Limitations in this network include the detection efficiency in Brazil, which is 70% in average (Naccarato et al., 2010) but can be significantly lower in areas with deficient coverage such as Northern Brazil, including the Amazon region, as well as the definition of a measured stroke as a single or multiple real return strokes (Murphy and Nag, 2015). Strokes data were accumulated over 12 minutes in the same timestamps as the radar data and selected within the clusters polygons delimited by TATHUthe tracking algorithm.

2.2 Tracking methodology

60

65

The convective systems database was created with the TATHU (Tracking and Analysis of Thunderstorms) software package (Uba et al., 2022) applied to the radar data described in the previous section. The software is a free, open-source python package available at https://github.com/uba/tathu, which addresses convective system tracking as a multi-target tracking problem (Makris and Prieur, 2014). The main modules are observation, detection, description, tracking, and forecast (not used in this study). The algorithm detects agglomerates of pixels – called herein **clusters** of storm cells – in an input field at a single time step according to the (one or more) threshold(s) and extracts its statistics such as size (in pixels), mean and maximum values

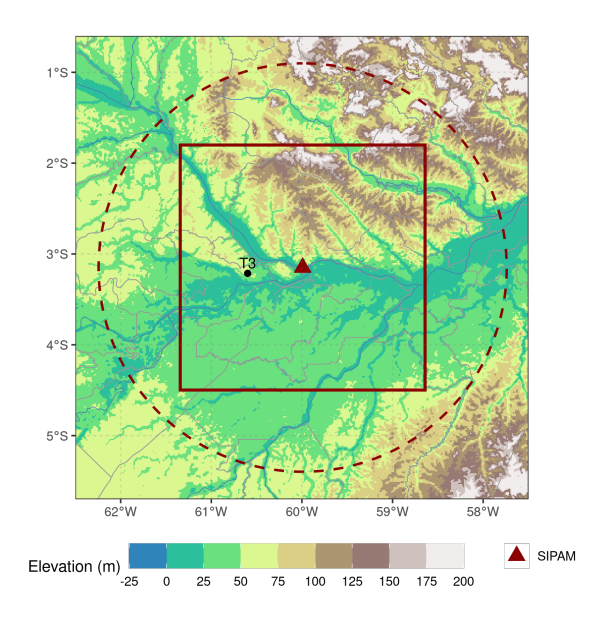


Figure 1. Amazonian region used in this study, with SIPAM radar location (red triangle), 250-km originally calculated coverage (dashed red lines), 150 km x 150 km bounding box (red square) used in the study and T3 site location in Manacapuru where surface data were collected (not shown in this study)

Table 1. SIPAM radar data settings processed by CPTEC-INPE

Туре	CAPPIs
Format	Binary, 15 x 500 x 500 elements
Resolution (vertical, horizontal, temporal)	1 x 1 x 1 km, 12 min
Min, max height	2 km, 16 km
CAPPI processing software	RSL (Radar Software Library)
Bias correction (Schumacher and Funk, 2018)	2014-01-03 to 2014-02-05: + 1.0 dB 2014-02-06 to 2014-08-19: + 3.0 dB 2014-08-20 to 2014-10-16: - 2.5 dB 2014-10-17 to 2015-03-06: - 5.5 dB 2015-03-07 to 2015-07-05: - 4.0 dB 2015-07-06 to 2015-10-28: - 1.5 dB 2015-10-29 to 2015-12-31: + 1.0 dB

of the input field, among others. From subsequent time steps, based on spatial overlap, it tracks and names (via a universal unique identifier — *uuid*) the **convective systems** that occurred in the period and its status during the described life cycle, with status being "spontaneous generation" (new cluster), "continuity" (growing or decaying cluster), "split" (when a single cluster separates into two or more clusters after a time step) or "merge" (when two or more clusters merge into a single cluster after a time step). The identification of a split or a merge depends mainly on the clusters propagation between subsequent time steps, where discrepancies can occur in situations such as clusters generating within the same relative overlap area of other propagating clusters. This split/merge problem is common to several tracking algorithms that use area overlap strategies, such as SCIT (The Storm Cell Identification and Tracking Algorithm, Johnson et al. (1998)) and TITAN (Thunderstorm Identification, Tracking, Analysis, and Nowcasting, Dixon and Wiener (1993)).

100

105

110

115

120

Table 2 shows the TATHU settings used in this study. We selected SIPAM radar reflectivity greater than 20 dBZ at the 3-km CAPPI field as the input field to the TATHU tracking algorithm based on several considerations. First, this altitude lies above the typical cloud base in the region (Fisch et al., 2004; Souza et al., 2023) and coincides with the level where maximum reflectivity is frequently observed in convective precipitation cores below freezing layer. Second, lower elevations near the radar are significantly affected by ground clutter and beam blockage (Giangrande et al., 2016; Schumacher and Funk, 2018), which compromises the reliability of reflectivity data closer to the surface. Additionally, the SIPAM radar's relatively coarse resolution limits the ability to resolve vertical structures accurately, particularly storm tilts. However, in the tropical environment of the Amazon, vertical wind shear is generally weak, reducing the likelihood of significant storm tilt or vertical displacement of convective cores. These factors together support the use of a horizontal 3-km CAPPI as a consistent and suitable input for identifying and tracking convective systems in this study. Other tracking algorithms consider composite reflectivity (e.g., Heikenfeld et al. (2019); Sokolowsky et al. (2024)) instead of 2D reflectivity fields to offer a more comprehensive depiction of the 3D structure of convective systems. However, considering the context of our study and the nature of this dataset just exposed above, the 3D structure of the convective systems should be captured. A comprehensive study of the implications for the reflectivity thresholds for tracking convective systems in CAPPI fields can be found in Leal et al. (2022), and it is not within the scope of this study. Moreover, our approach is consistent methodologically with previous studies that have successfully employed single-level CAPPI fields to characterize convective systems in the Amazon (e.g., Laurent and Laurent (2002); Albrecht et al. (2011); Leal et al. (2022); Gupta et al. (2024)). These studies provided valuable insights into storm morphology, evolution, and vertical structure using similar techniques. Adopting a comparable methodology ensures continuity and comparability with the existing body of literature on Amazonian convection.

The relative overlap area strategy considers two subsequent clusters in time as the same convective system when there 's is at least a 10% overlap between their areas (i.e., polygons). The maximum interval between images considers a data gap sufficient to ensure continuity of the convective systems, but can result in different convective systems being tracked as the same if they are in the overlap area, considering that the average lifecycle of tropical convection is smaller than 60 minutes. Within the main statistics, the clusters with number of threshold layers equal to "0" (for only having the 20-dBZ reflectivity threshold) or "1" (for having both 20 and 40-dBZ reflectivity thresholds), can be used to separate systems with or without deep convective cores.

Table 2. TATHU parameters (original names in parentheses) and values chosen for the generation of *systems* (raw) and *systems_filtered* (filtered) datasets.

Input data	3-km CAPPI in a 150 x 150 km box (300 x 300 elements) centered at the radar location, between January 2014 and December 2015
Reflectivity thresholds (threshold value)	values greater than 20 dBZ, 40 dBZ
Minimum cluster sizes (minarea)	$100 \text{ km}^2, 40 \text{ km}^2$
Tracking technique (trackers class)	Relative overlap area (RelativeOverlapAreaStrategy)
Minimum cluster overlap area	10%
Maximum interval between images	60 min
Statistics (stats)	Maximum, mean and standard deviation of reflectivity, size (amount of pixels), number of layers (corresponding to having one or two reflectivity and minimum size thresholds)
Output	PostGIS database (systems and systems_filtered tables)
Filters applied	 Have at least one 40 dBZ/40 km² (corresponding to deep convection) pixel in any timestamp Do not intersect the bounding box of the grid (corresponding to probably have part of the cluster outside the tracking region) Last longer than 12 minutes (one timestamp) or have relation with other convective system (by split or merge)

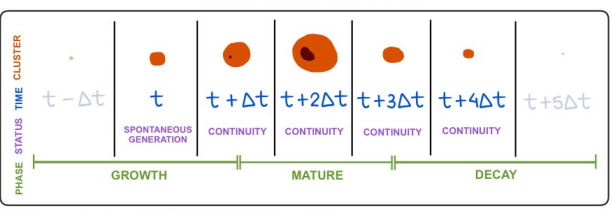
For better illustration of the terminology of TATHU tracking system applied to SIPAM 3-km CAPPI fields, Fig. 2 shows a schematic of these definitions: a **cluster** is a contiguous region (polygon) of pixels within the 3-km CAPPI reflectivity field that exceeds 20 dBZ reflectivity threshold *identified at a single time step*; a **convective system** is a time-continuous sequence of clusters that are linked across radar volumes based on spatial overlap. A **cluster** can have one or several cores that exceed 40 dBZ reflectivity threshold, an estimation of deep convection, but these cores are not considered as separated clusters considered as part of a single cluster during the description and tracking of the convective systems.

Output data was stored in a PostGIS database, a Data Base Management System (DBMS) with geospatial support that allows storage of large volumes of data in tabular form, including geolocated geometries. The database was converted to GeoJSON datasets in order to become easily available at Lopes (2024).

130

Two datasets were defined based on the TATHU tracking. The original - called herein **raw** - dataset contains all the convective systems observed in the period, regardless of duration, size and status during the life cycle. The **filtered** dataset contains only the convective systems that met the filtering criteria described in Table 2. The second threshold criteria (40 dBZ in a 40 km²)

CONVECTIVE SYSTEM



Cluster morphology with 20 dBZ, 40 dBZ thresholds Convective system lifecycle, status, phase

Figure 2. Illustrative deep convective system as observed by TATHU: clusters morphology with 20-dBZ (orange) and 40-dBZ (dark red) thresholds in 5 <u>valid</u> subsequent timestamps with TATHU status (spontaneous generation or continuity) and different phases (growth, mature and decay) of a full lifecycle.

minimum area) is used here as a definition of deep convective cores present during the lifecycle. Clusters intersecting the borders of the grid had their associated convective systems discarded to exclude systems without full lifecycle within the study area. Systems with only one timestep were also discarded. We created this filtered dataset to provide a subset of deep convective systems with full life cycle, important criteria for several convection studies.

The original *systems* dataset contains 91609 convective systems and 322896 clusters, while the filtered *systems_filtered* dataset contains 5976 convective systems (6.5% of the original dataset) and 40394 clusters (12.5% of the original dataset). Using the filtered dataset with the additional lightning data, several other parameters were calculated for each cluster (Table 3) related to storm morphology. The following equations were applied for VIWL (Vertically Integrated Warm Liquid), VII (Vertically Integrated Ice) and VIL (Vertically Integrated Liquid), respectively:

$$VIWL = \sum_{i=2km}^{5km} 3.44 \times 10^{-6} \left(\frac{Z_i + Z_{i+1}}{2} \right)^{\frac{4}{7}}$$
 (1)

145
$$VII = \sum_{i=7km}^{16km} \pi \rho_i N_o^{\frac{3}{7}} \left[\frac{5.28 \times 10^{-18}}{720} \left(\frac{Z_i + Z_{i+1}}{2} \right) \right]^{\frac{4}{7}}$$
 (2)

$$VIL = \sum_{i=2km}^{16km} 3.44 \times 10^{-6} \left(\frac{Z_i + Z_{i+1}}{2} \right)^{\frac{4}{7}}$$
 (3)

3 Results

3.1 Raw and filtered datasets characteristics

This subsection compares the physical characteristics between the raw and filtered datasets in order to define what type of convective system each dataset represents. Fig. 3 shows the size — represented by area in km² — distribution of clusters

Table 3. Clusters additional parameters calculated on the filtered dataset

Variable	Description	Reference
gld	GLD strokes within cluster area detected within 12 min (interval between scans)	
echotop_0, echotop_20, echotop_40	0, 20 and 40 dBZ echo top heights	
z_freq	Reflectivity frequencies per height; 15 x 16 matrices with reflectivities between -10 and 70 dBZ (every 5 dBZ) and heights between 2 and 16 km	Yuter and Houze (1995)
viwl_kgm2	VIWL (Vertically Integrated Warm Liquid) of cluster in kg/m ² , Equation 1	
vii_kgm2	VII (Vertically Integrated Ice) of clusters in kg/m², Equation 2	Petersen and Rutledge (2001)
vil_kgm2	VIL (Vertically Integrated Liquid) of cluster in kg/m², Equation 3	Greene and Clark (1972)
nae_s_1	Normalized area expansion in $\rm s^{-1}$ between clusters of a same convective system	Machado and Laurent (2004)
gld_strmin	Strokes rate between clusters of a same convective system in strokes/min	
echotop0_kmmin, echotop20_kmmin, echotop40_kmmin	0, 20 and 40 dBZ echo top rate between clusters of a same convective system in km/min	

and maximum size of convective systems. Both distributions have maximum frequency in the smallest (1000 km²) area. The maximum area of the raw systems is 6 times larger (60000 km² vs 10000 km²) and the distribution drops faster in the filtered systems. These characteristics show the filtering effect around the border of the 150 km bounding box (Fig. 1), which excluded very large clusters: a. A 200 × 200 points clusters with a 40000 km² area, for example, can be considered too large because it occupies 2/3 of the grid and probably intercepts the border of the bounding box in a given time stamp.

Fig. 4 shows the mean and maximum clusters reflectivity distribution of raw (a) and filtered (b) datasets. On raw data, the distributions show no significant frequency peaks, with mean reflectivity distributed mainly (frequency above 20%) between 20 and 40 dBZ and maximum reflectivity between 35 and 50 dBZ (frequency above 15%). Oppositely, on the filtered data, peaks (above 35%) can be found between 25 and 40 dBZ and between 50 and 55 dBZ of mean and maximum reflectivity,

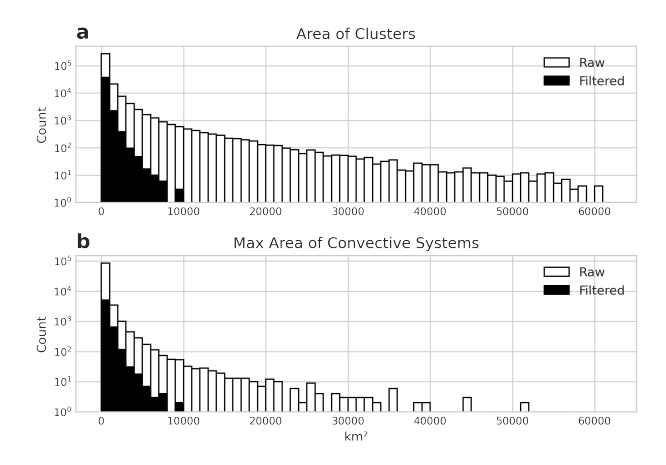


Figure 3. Distribution of clusters area (a) and convective systems' max area (b) of raw (white) and filtered (black) datasets.

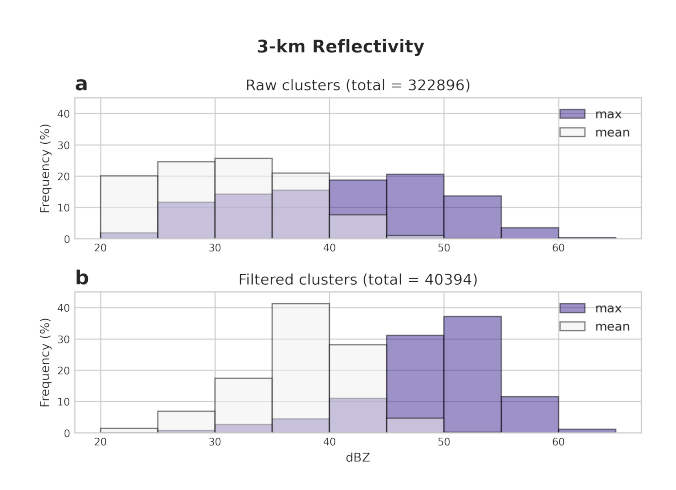


Figure 4. Distribution of clusters max (purple) and mean (white) reflectivity of raw (a) and filtered (b) datasets.

respectively. These differences between the distributions represent the filtering effect on the type of the selected clusters: the the filters ended up selecting more intense clusters (larger mean and maximum reflectivity) and excluded mainly the ones that did not exceed 40 dBZ — observe that the clusters with maximum reflectivity below 40 dBZ are significantly less frequent (below 5%) compared to the raw data ones.

Table 4 shows some characteristics of the convective systems of raw and filtered datasets using the clusters classifications on each time step. On both datasets, the percentage of spontaneously generated convective systems was similar (above 70%); on the raw data, not all these systems had their full lifecycle covered, while on the filtered data this is true because one of the filtering criteria is to exclude convective systems that leave the radar coverage area. 53% of the filtered convective systems had split or merge during their lifecycle, compared to 37% of the raw systems; an important point here is that 31% of the

Table 4. Frequency of spontaneously generated (did not generate from splits or first steps of algorithm rounds), with split and/or merge and full lifecycle (last time step in continuity) convective systems (CS) of raw and filtered datasets.

	Raw	Filtered
Convective Systems (total)	91609	5976
CS spontaneously generated (%)	72	73
CS with split/merge (%)	37	53
CS with full lifecycle (%)	49	80

raw systems and only 2% of the filtered systems lasted only one time step (12 min) (not shown), meaning that raw convective systems did not last long enough to go through split or merge. The majority (80%) of the filtered and half (49%) of the raw convective systems were considered with full lifecycle (last time step was "continuity"), which also is explained by the high percentage of raw systems with only one time step (i.e., only "spontaneous generation" status). The 20% of filtered convective systems without full lifecycle are within the not spontaneously generated systems, products of split or merge of other systems.

170

175

180

190

Table 5 shows the distribution of convective systems durations of raw and filtered data datasets. The majority of raw (40%) and filtered (47%) systems lasted up to 1 hour, indicating the predominance of isolated convective systems (Giangrande et al., 2023; Viscardi et al., 2024; Gupta et al., 2024). Only 10% of raw systems lasted between 1 and 3h, compared to 36% of filtered systems. The majority of convective systems were short-lived, with 40% of raw and 47% of filtered systems lasting up to 1 hour, highlighting the prevalence of isolated convective systems. A notable difference is observed in the 1–3h range, where only 10% of raw systems persisted, compared to 36% in the filtered dataset. For long-duration systems, a significant disparity emerges: nearly twice as many raw systems (631) lasted longer than 6h compared to those in the 5–6h range (318). In contrast, the filtered dataset shows fewer systems exceeding 6h (18) than those lasting between 5–6h (27), indicating a stronger filtering effect effect of the area filtering on prolonged convective systems.

Fig. 5 shows the monthly distribution of raw and filtered clusters and convective systems. Seasons and intensive operation periods (IOPs) were defined according to Machado et al. (2018): dry season between August and October, dry-to-wet season between November and December, wet season between January and March, IOP1 between February 1st and March 31st 2014 and IOP2 between August 15th and October 15th 2014. In general, a larger frequency of clusters and convective systems occurred in the wet and transition (wet-to-dry and dry-to-wet) seasons, with a peak of filtered clusters/systems in November 2015 (almost two times more than the raw clusters/systems). The proportion between raw and filtered systems changes over the months, with a larger frequency of raw clusters and convective systems on the wet seasons and the opposite on the dry seasons. This difference can be explained by the filter of very large clusters cited previously, which are more common in the wet season. Considering the climatological characteristics of each season, it is expected that more clusters/convective systems occur during the wet season than of the dry season, which was the case for both raw and filtered data.

Table 5. Frequency of spontaneously generated (did not generate from splits or first steps of algorithm rounds), with split and/or merge and full lifecycle (last time step in continuity) convective systems (CS) of raw and filtered data tables.

	Raw	Filtered
CS duration $\leq 1h$	79301 (86,6%)	3448 (57,7%)
$1h < CS $ duration $\leq 2h$	6950 (7,6%)	1535 (25,7%)
$2h < CS $ duration $\leq 3h$	2597 (2,8%)	635 (10,6%)
$3h < CS $ duration $\leq 4h$	1170 (1,3%)	239 (4%)
$4h < CS $ duration $\leq 5h$	641 (0,7%)	74 (1,2%)
$5h < CS $ duration $\leq 6h$	318 (0,3%)	27 (0,5%)
CS duration > 6h	631 (0,6%)	18 (0,3%)
Total	91609 (100%)	5976 (100%)

Monthly distributions Clusters Raw (total = 322896) Filtered (total = 40394) Nov 2014 Dec 2014 Jan 201-May 2014 Oct 2014 Jan 201 Feb 2015 Jun 201 Aug 201 Sep 201 Apr 201 Aug 201 Jul 201 May 201 Jun 201 b Convective Systems Raw (total = 91609) Filtered (total = 5976) Wet season Dry season

Figure 5. Monthly relative frequency distribution of clusters (a) and convective systems (b) of raw (white) and filtered (black) datasets. The blue and red areas delimit wet and dry seasons, respectively, and dashed lines delimit the intensive operation periods IOP1 and IOP2.

Table 6 presents the duration of raw and filtered convective systems by IOP. The distribution of system durations is generally consistent across seasons, with similar proportions observed between raw and filtered datasets. In contrast to Table 5, where

Table 6. Distribution of convective systems (CS) durations of raw and filtered datasets separated by intensive operation periods IOP1 and IOP2.

	IOP1		IOP2	
	Raw	Filtered	Raw	Filtered
CS duration $\leq 1h$	8427 (86,1%)	176 (55,7%)	6565 (90%)	272 (55,5%)
$1h < CS $ duration $\leq 2h$	772 (7,9%)	88 (27,8%)	432 (5,9%)	130 (26,5%)
$2h < CS $ duration $\leq 3h$	277 (2,8%)	34 (10,8%)	146 (2%)	53 (10,8%)
$3h < CS $ duration $\leq 4h$	118 (1,2%)	10 (3,2%)	60 (0,8%)	24 (4,9%)
$4h < CS $ duration $\leq 5h$	66 (0,7%)	6 (1,9%)	41 (0,6%)	7 (1,4%)
$5h < CS $ duration $\leq 6h$	40 (0,4%)	0 (0%)	19 (0,3%)	2 (0,4%)
CS duration $\geq 6h$	91 (0,9%)	2 (0,6%)	31 (0,4%)	2 (0,4%)
Total	9792 (100%)	316 (100%)	7294 (100%)	490 (100%)

less than half of the raw systems lasted up to 1h, seasonal distributions show that more than 80% of raw systems and 50% of filtered systems persisted for no more than 1h, indicating the predominance of isolated convective systems. Additionally, 97% of raw and 94% of filtered systems had durations of 3h or less.

Fig. 6 shows the hourly distribution of raw and filtered clusters divided by IOP. Comparing the raw and filtered clusters, in all seasons there are a larger frequency of raw clusters during late night/dawn and a larger frequency of filtered clusters during late morning/afternoon. In the dry season (IOP2), this difference is more pronounced: the filtered clusters are more frequent (above 15%) between 1400 and 1500 local time compared to the raw clusters (below 10%), while the raw clusters are 5% more frequent than the filtered clusters between 2300 and 0700 local time. These differences between raw and filtered clusters indicate a more diurnal characteristic of the filtered clusters, while the raw clusters are more nocturnal, probably represented by the very large and long-lasting (above 6h) clusters described previously.

200

205

210

Fig. 7 shows the hourly distribution of raw and filtered convective systems initiation (defined here as the first timestamp) divided by IOP. Comparing the raw and filtered systems, in both seasons there are a larger frequency of raw systems initiating during dawn, while a larger frequency of filtered systems initiate during morning/afternoon. This difference is even greater (almost 10%) in the dry season. Comparing the seasons, both in the dry and wet seasons the initiation peak occurs only at 1400 local time. Specifically about the filtered systems, the 1400 local time peak during the wet season is not highlighted in IOP1, with another peak at 1200 local time.

When comparing the physical characteristics of the raw and filtered datasets, the filters significantly decrease the sampling size yet defines a specific subset of convective systems: in general, they have areas up to 10000 km², maximum reflectivity

Hourly distribution of clusters

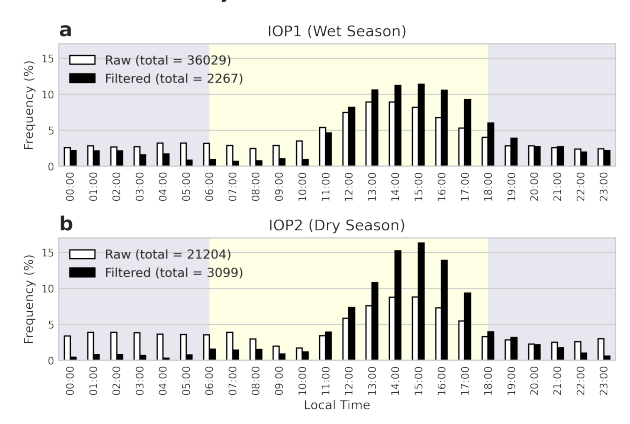
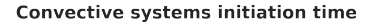


Figure 6. Hourly relative distribution of clusters of raw (white) and filtered (black) datasets separated by intensive operation periods IOP1 (a) and IOP2 (b). The blue and yellow areas delimit diurnal and nocturnal periods, respectively.



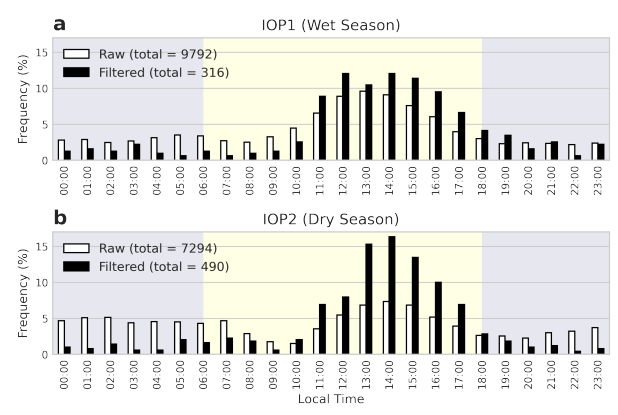


Figure 7. Hourly relative distribution of convective systems initiation time of raw (white) and filtered (black) datasets separated by intensive operation periods IOP1 (a) and IOP2 (b). The blue and yellow areas delimit diurnal and nocturnal periods, respectively.

mainly above 50 dBZ, full lifecycle (growth, mature and decay phases) and last up to 3h. The raw dataset includes these same systems as well as diverse convective types such as mesoscale (considering the areas above 50000 km²), both short-lived (12 min duration) and long-lived (duration above 6h), and stratiform (reflectivity below 30 dBZ) systems. Both datasets are useful in further convection studies but should be chosen rigorously depending on their objectives: if. If the convection phase is important, for example, the filtered dataset will be more appropriate, while some studies can benefit from convection patterns in the Amazon region that can be extracted from the raw dataset.

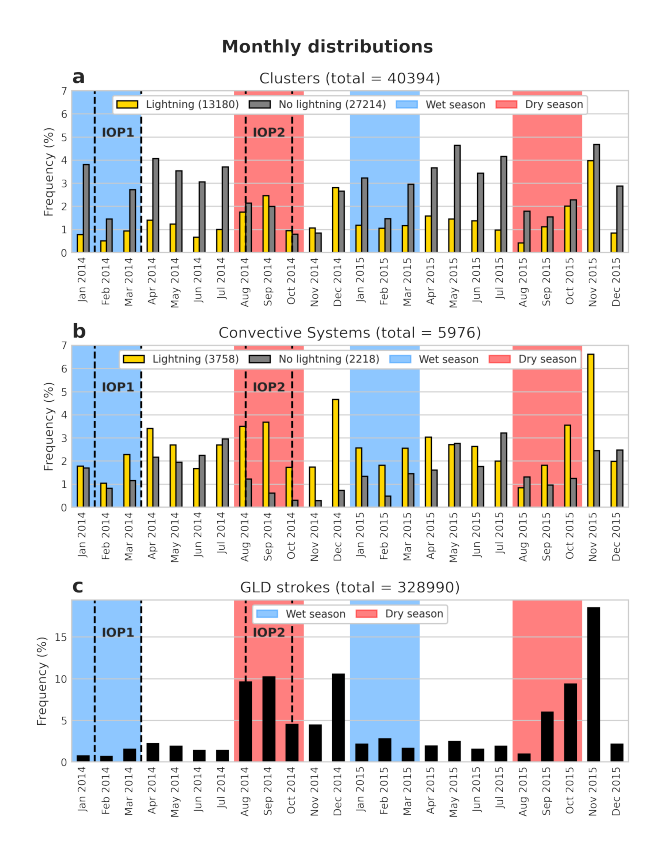


Figure 8. Monthly relative distribution of clusters (a), convective systems (b) and GLD strokes (c) of filtered datasets separated by lightning (yellow bars) or no lightning (gray bars) occurrence. The blue and red areas delimit wet and dry seasons, respectively, and dashed lines delimit the intensive operation periods IOP1 and IOP2.

3.2 Characteristics specific to the filtered systems

Starting with the monthly distribution, Fig. 8 shows the clusters and convective systems separated by lightning activity, as well as the distribution of GLD strokes. More than double the clusters (27214 vs. 13180) had no electrical activity, while more convective systems (3758 vs. 2218) showed lightning, which means that, in general, the convective systems with lightning consists of only a few clusters with lightning. There are significant differences between clusters and systems frequency: a A larger frequency of clusters and systems without lightning occurs between wet and dry seasons, while peaks of clusters and systems frequency occurs in the dry-to-wet season, comparable to the peak strokes frequency. These findings are similar to what is found in previous works such as Albrecht et al. (2011, 2016).

Separating the analysis in systems with and without lightning, Fig. 9 shows the hourly distribution of clusters and initiation (first timestamp) of convective systems with lightning and GLD strokes separated by IOP. All variables are more frequent during late morning/afternoon, with significant differences between IOPs: on IOP2, the clusters and strokes peaks oc-

Hourly distribution per IOP

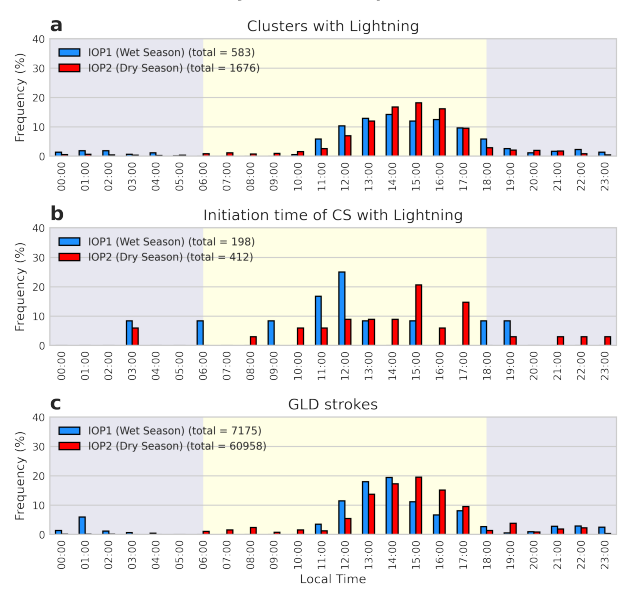


Figure 9. Hourly relative distribution of clusters with lightning (a), initiation time of clusters with lightning (b) and GLD strokes (c) of filtered dataset during intensive operation periods IOP1 (blue) and IOP2 (red). The blue and yellow areas delimit diurnal and nocturnal periods, respectively.

curs at 1500 local time, which is also the preferential time of convective systems initiation; on. On IOP1, the clusters cluster and strokes peaks occur around the same time, but the systems initiation occurs preferentially earlier, at 1200 local time. It's important to note that the The low amount of systems (198 on IOP1 and 412 on IOP2) influenced the frequency distribution, but the results were similar to their corresponding dry and wet seasons (not shown). For the clusters and initiation of convective Convective systems without lightning (not shown), the largest frequencies occur are more frequent during late morning/after-noon (not shown). The initiation frequency peaks on the dry and wet seasons occur at 1500 local time, while on the dry-to-wet season the distribution is more dispersed, with approximately equal peaks at 1200, 1300 e 1600 local time.

In order to analyze the propagation direction of the convective systems, Fig. 10 shows the frequency distribution of the propagation direction separated by IOP. The predominant direction of the convective systems is from the east, consistent with the main dynamic forcing in the Amazon: moisture flux from the tropical Atlantic by the easterlies influenced by the position of the Intertropical Convergence Zone (ITCZ) (Silva Dias and Carvalho, 2016). Comparing the IOPs, in the wet season, about 25% propagated from the east and east-northeast, while in the dry season more than 30% of the systems propagated from the east and east-southeast. This direction shift from east-northeast to east-southeast is related to the shift in the position of the ITCZ and the cold fronts propagation in the South American continent, which affect the zonal winds regime in the Amazonian region (Rickenbach et al., 2002). These results are also consistent with Gupta et al. (2024), which focused on isolated convective systems near Manacapuru (T3) site.

240

Propagation Direction of Convective Systems

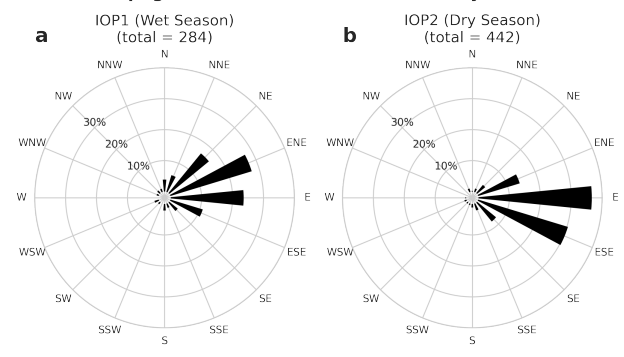


Figure 10. Convective systems' relative propagation direction distribution in the filtered dataset separated by intensive operation periods IOP1 (a) and IOP2 (b). The direction was defined by the distance between the first and last centroids of the convective system.

In order to analyze the intensity of the convective systems, Fig. 11 shows the frequency distribution of maximum heights and variation rates (considering the 12-min interval between radar scans) of the 0, 20 and 40 dBZ echoes, associated with the cloud top height, precipitable hydrometeors height and intense precipitation heights, respectively. The maximum top heights are more frequent above 10 km, with peaks in 11 km (dry season) and 15 km (wet season). The maximum precipitable height was more frequent between 7 and 11 km. The maximum intense precipitation height was also more frequent between 4 and 7 km, with peaks in 5 km (both dry and wet seasons). These high tops, complemented by maximum precipitation height more frequently between 7 and 11 km and maximum intense precipitation height more frequently between 4 and 7 km, show how these systems were predominantly deep in its most intense moment. The variation rates (Fig. 11b) were similar between the echoes, with frequency peaks in -0,2 and 0,2 km/min, indicating significant fluctuations of the echo tops throughout its life cycle.

250

255

260

Fig. 12 shows the frequency distribution of the maximum echo tops of 0, 20 and 40 dBZ separated by IOPs to IOP. As in the complete time series, the maximum top heights are more frequent above 10 km, with peaks in 11 km (IOP2) and 15 km (IOP1). The maximum precipitable height was also more frequent between 7 and 11 km. The maximum intense precipitation height was also more frequent between 4 and 7 km, with peaks in 5 km.

In order to analyze the clusters vertical profile, Fig. 13 shows the frequency diagram by altitude of the clusters reflectivity of the complete time series. The most frequent profile is of a small reflectivity variation with height, 25 dBZ on the surface to 10 dBZ on 15 km height (i.e., a -1 dBZ per km variation rate). Less frequent (between 5 and 10%) profiles have very low (5 to 10 dBZ) or high (40 dBZ) reflectivity on the surface, and up to 25 dBZ on 15 km height, with a minimum of 0 dBZ on 12 km height.

Fig. 14 shows the clusters frequency by altitude diagram separated by IOP as well the different between them. Considering the largest frequencies, the profiles are similar between them (and with the complete time series profile), but the IOP1 profile (wet season) is more intense (up to 20%) than the IOP2 (dry season), specially between 10 and 20 dBZ.

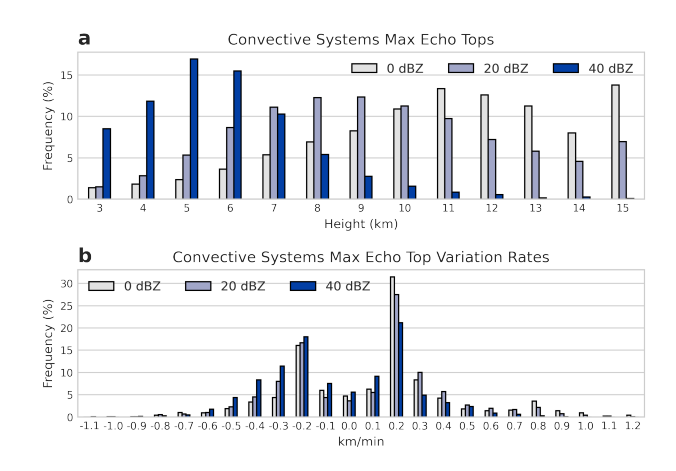


Figure 11. Convective systems' 0 (gray bars), 20 (light blue bars) and 40 dBZ (dark blue bars) max echo tops (a) and variation rates (b).

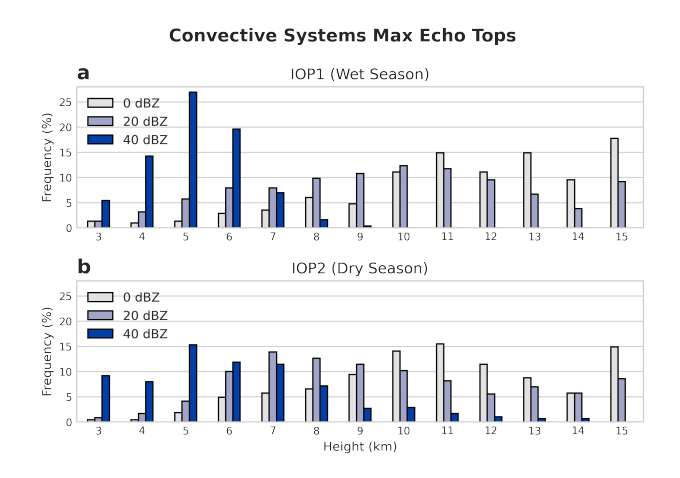


Figure 12. Convective systems' 0 (gray bars), 20 (light blue bars) and 40 dBZ (dark blue bars) max echo tops separated by intensive operation periods IOP1 (a) and IOP2 (b).

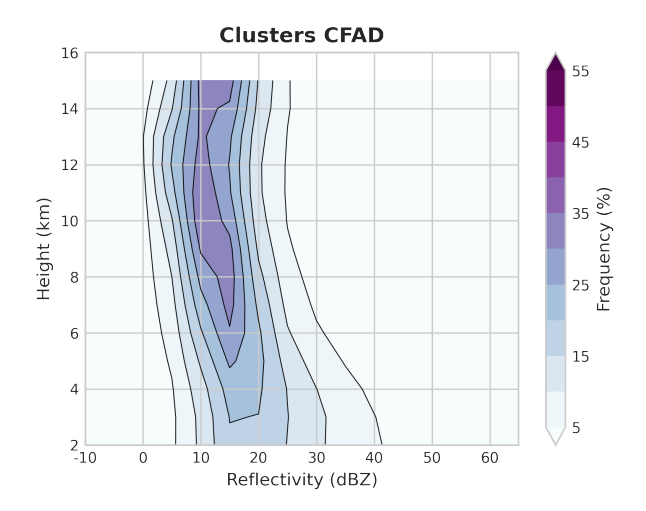


Figure 13. Mean Contoured Frequency by Altitude Diagram (CFAD) of clusters' reflectivity with 5-dBZ bins.

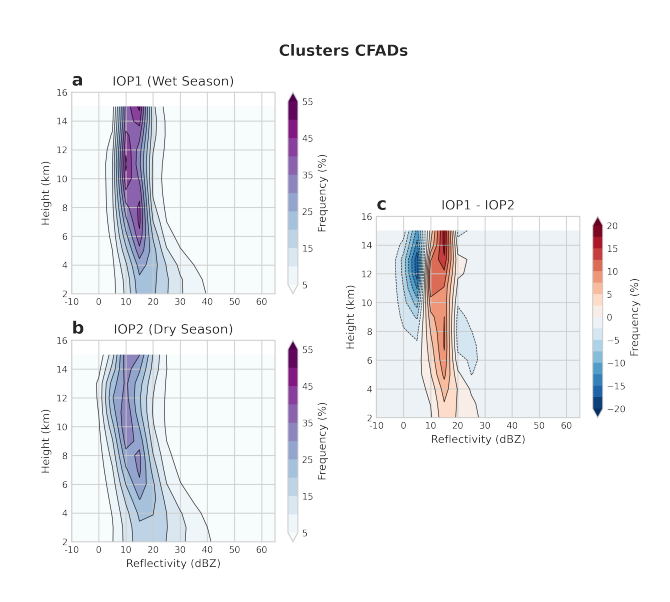


Figure 14. Mean Contoured Frequency by Altitude Diagram (CFAD) of clusters' reflectivity with 5-dBZ bins separated by intensive operation periods IOP1 (a) and IOP2 (b) as well as IOP1 - IOP2 anomaly (c).

4 Conclusions

A database of convective systems that occurred during GoAmazon experiment was created to provide comprehensive convection data for future GoAmazon studies. The *systems* and *systems_filtered* datasets cover the main convective characteristics, including morphology and intensity, as well as electrical activity. The filtered dataset is shown to be an acceptable sample of the complete dataset, selecting deep convective systems with full lifecycle within the research area. Convection seasonality is also well represented, with more intense convective systems between dry and dry-to-wet seasons and less intense in the wet season, typically occurring during late morning/early afternoon. The preeminent propagation direction of these systems are associated with easterlies with a transition from slightly north to slightly south associated with the ITCZ position.

It is important to consider the limitations in the convection description when using these data for future research. Since the SIPAM radar main role is operational, its settings are not optimal for convection research: low spatial (1 km) and temporal (12 min) resolution (considering it is a weather radar), beam blockage during the experiment (Giangrande et al., 2016; Tian et al., 2021), radar software settings change during the experiment. Another limitation is in the tracking itself, specially when dealing with system split/merge (which occurs in a significant portion of the convective systems database) that can be more complex in large, mesoscale systems. Even with these limitations, the database is an important source of convection characteristics for cloud-aerosol-precipitation research.

5 Code availability

280

The TATHU software package is available at https://github.com/uba/tathu (Uba et al., 2022). The code developed to create the datasets with TATHU is available at https://github.com/cclopes/tathu/tree/sipam-tracking/sipam-tracking.

6 Data availability

The *systems* and *systems_filtered* datasets are available at https://doi.org/10.5281/zenodo.13732692 (Lopes, 2024). SIPAM radar data are available at https://ftp.cptec.inpe.br/chuva/goamazon/experimental/level_0/eq_radar/esp_band_s/st_sipam/.

Author contributions. CL and RA designed the study. CL processed the data and wrote the manuscript advised by RA. DU developed the tracking software, helped during data processing, and reviewed the manuscript. TB processed the radar data and reviewed the manuscript. IS helped in providing the radar data and reviewed the manuscript.

Competing interests. No competing interests are present.

Acknowledgements. This study was funded by Coordenação de Aperfeiçoamento de Pessoal de Nível Superior (CAPES - grant 88887.464412/2019-00), Fundação de Amparo à Pesquisa do Estado de São Paulo (Fapesp - grants 2009/15235-8, 2017/17047-0, 2022/13257-9, 2023/04358-9) and Conselho Nacional de Desenvolvimento Científico e Tecnológico (CNPq - grants 438638/2018-2, 313355/2021-5, 440171/2022-9). We would like to thank Sistema de Proteção da Amazônia (SIPAM) for providing the radar data and the ARM GoAmazon 2014/5 operations and science team for their efforts during the experiment. We also thank Vaisala Inc. for providing the GLD360 lightning dataset for this study.

References

- Albrecht, R. I., Morales, C. A., and Dias, M. A. F. S.: Electrification of precipitating systems over the Amazon: Physical processes of thunderstorm development, Journal of Geophysical Research, D: Atmospheres, 116, D08 209, https://doi.org/10.1029/2010jd014756, 2011.
 - Albrecht, R. I., Goodman, S. J., Buechler, D. E., Blakeslee, R. J., Christian, H. J., Albrecht, R. I., Goodman, S. J., Buechler, D. E., Blakeslee, R. J., and Christian, H. J.: Where are the lightning hotspots on Earth?, Bulletin of the American Meteorological Society, 97, BAMS–D–14–00 193.1, https://doi.org/10.1175/bams-d-14-00193.1, 2016.
- Artaxo, P., Hansson, H. C., Machado, L. A. T., and Rizzo, L. V.: Tropical forests are crucial in regulating the climate on Earth, PLOS Climate, 1, e0000 054, https://doi.org/10.1371/journal.pclm.0000054, 2022.
 - Biscaro, T. S., Machado, L. A. T., Giangrande, S. E., and Jensen, M. P.: What drives daily precipitation over the central Amazon? Differences observed between wet and dry seasons, Atmospheric Chemistry and Physics, 21, 6735–6754, https://doi.org/10.5194/acp-21-6735-2021, 2021.
- Demetriades, N. W. S., Murphy, M. J., and Cramer, J. A.: Validation of Vaisala's global lightning dataset (GLD360) over the continental

 United States, in: Preprints, 29th Conf. on Hurricanes and Tropical Meteorology, Tucson, AZ, Amer. Meteor. Soc. D, vol. 16, vaisala.com, https://www.vaisala.com/sites/default/files/documents/6.Demetriades, %20Murphy, %20Cramer.pdf, 2010.
 - Dixon, M. and Wiener, G.: TITAN: Thunderstorm Identification, Tracking, Analysis, and Nowcasting—A Radar-based Methodology, Journal of Atmospheric and Oceanic Technology, 10, 785–797, https://doi.org/10.1175/1520-0426(1993)010<0785:TTITAA>2.0.CO;2, 1993.
- Fisch, G., Tota, J., Machado, L. A. T., Silva Dias, M. A. F., da F. Lyra, R. F., Nobre, C. A., Dolman, A. J., and Gash, J. H. C.: The convective boundary layer over pasture and forest in Amazonia, Theoretical and applied climatology, 78, 47–59, https://doi.org/10.1007/s00704-004-0043-x, 2004.
 - Giangrande, S. E., Toto, T., Jensen, M. P., Bartholomew, M. J., Feng, Z., Protat, A., Williams, C. R., Schumacher, C., and Machado, L.: Convective cloud vertical velocity and mass-flux characteristics from radar wind profiler observations during GoAmazon2014/5, Journal of Geophysical Research, D: Atmospheres, 121, 12,891–12,913, https://doi.org/10.1002/2016JD025303, 2016.
- Giangrande, S. E., Feng, Z., Jensen, M. P., Comstock, J. M., Johnson, K. L., Toto, T., Wang, M., Burleyson, C., Bharadwaj, N., Mei, F., Machado, L. A. T., Manzi, A. O., Xie, S., Tang, S., Silva Dias, M. A. F., de Souza, R. A. F., Schumacher, C., and Martin, S. T.: Cloud characteristics, thermodynamic controls and radiative impacts during the Observations and Modeling of the Green Ocean Amazon (GoAmazon2014/5) experiment, Atmospheric Chemistry and Physics, 17, 14519–14541, https://doi.org/10.5194/acp-17-14519-2017, 2017.
- Giangrande, S. E., Wang, D., and Mechem, D. B.: Cloud regimes over the Amazon Basin: perspectives from the GoAmazon2014/5 campaign, Atmospheric Chemistry and Physics, 20, 7489–7507, https://doi.org/10.5194/acp-20-7489-2020, 2020.
 - Giangrande, S. E., Biscaro, T. S., and Peters, J. M.: Seasonal controls on isolated convective storm drafts, precipitation intensity, and life cycle as observed during GoAmazon2014/5, Atmospheric chemistry and physics, 23, 5297–5316, https://doi.org/10.5194/acp-23-5297-2023, 2023.
- 330 Greene, D. R. and Clark, R. A.: Vertically Integrated Liquid Water—A New Analysis Tool, Monthly Weather Review, 100, 548–552, https://doi.org/10.1175/1520-0493(1972)100<0548:VILWNA>2.3.CO;2, 1972.
 - Gupta, S., Wang, D., Giangrande, S., Biscaro, T., and Jensen, M. P.: Lifecycle of updrafts and mass flux in isolated deep convection over the Amazon rainforest: insights from cell tracking, Atmospheric chemistry and physics, 24, 4487–4510, https://doi.org/10.5194/acp-24-4487-2024, 2024.

Harriss, R. C., Wofsy, S. C., Garstang, M., Browell, E. V., Molion, L. C. B., McNeal, R. J., Hoell, Jr, J. M., Bendura, R. J., Beck, S. M., Navarro, R. L., Riley, J. T., and Snell, R. L.: The Amazon Boundary Layer Experiment (ABLE 2A): dry season 1985, Journal of geophysical research, 93, 1351, https://doi.org/10.1029/jd093id02p01351, 1988.

340

350

- Harriss, R. C., Garstang, M., Wofsy, S. C., Beck, S. M., Bendura, R. J., Coelho, J. R. B., Drewry, J. W., Hoell, Jr, J. M., Matson, P. A., McNeal, R. J., Molion, L. C. B., Navarro, R. L., Rabine, V., and Snell, R. L.: The Amazon Boundary Layer Experiment: Wet season 1987, Journal of geophysical research, 95, 16721–16736, https://doi.org/10.1029/jd095id10p16721, 1990.
- Heikenfeld, M., Marinescu, P. J., Christensen, M., Watson-Parris, D., Senf, F., van den Heever, S. C., and Stier, P.: Tobac v1.0: Towards a flexible framework for tracking and analysis of clouds in diverse datasets, Geoscientific model development discussions, pp. 1–31, https://doi.org/10.5194/gmd-2019-105, 2019.
- Johnson, J. T., MacKeen, P. L., Witt, A., Mitchell, E. D. W., Stumpf, G. J., Eilts, M. D., and Thomas, K. W.: The Storm Cell Identification and Tracking Algorithm: An Enhanced WSR-88D Algorithm, Weather and Forecasting, 13, 263–276, https://doi.org/10.1175/1520-0434(1998)013<0263:tsciat>2.0.co; 2, 1998.
 - Jones, C. and Carvalho, L.: Active and break phases in the South American monsoon system, Journal of Climate, 15, 905–914, https://doi.org/10.1175/1520-0442(2002)015<0905:AABPIT>2.0.CO:2, 2002.
 - Laurent, H. and Laurent, D.: Characteristics of the Amazonian mesoscale convective systems observed from satellite and radar during the WETAMC/LBA experiment, Journal of Geophysical Research, https://doi.org/10.1029/2001JD000337, 2002.
 - Leal, H. B., Calheiros, A. J. P., Barbosa, H. M. J., Almeida, A. P., Sanchez, A., Vila, D. A., Garcia, S. R., and Macau, E. E. N.: Impact of Multi-Thresholds and Vector Correction for Tracking Precipitating Systems over the Amazon Basin, Remote Sensing, 14, 5408, https://doi.org/10.3390/rs14215408, 2022.
 - Lopes, C.: GoAmazon convective systems datasets (systems and systems_filtered), https://doi.org/10.5281/ZENODO.13732692, 2024.
- Machado, L. A. T. and Laurent, H.: The Convective System Area Expansion over Amazonia and Its Relationships with Convective System Life Duration and High-Level Wind Divergence, Monthly Weather Review, 132, 714–725, https://doi.org/10.1175/1520-0493(2004)132<0714:TCSAEO>2.0.CO;2, 2004.
 - Machado, L. A. T., Dias, M. A. F. S., Morales, C., Fisch, G., Vila, D., Albrecht, R., Goodman, S. J., Calheiros, A. J. P., Biscaro, T., Kummerow, C., Cohen, J., Fitzjarrald, D., Nascimento, E. L., Sakamoto, M. S., Cunningham, C., Chaboureau, J.-P., Petersen, W. A., Adams, D. K., Baldini, L., Angelis, C. F., Sapucci, L. F., Salio, P., Barbosa, H. M. J., Landulfo, E., Souza, R. A. F., Blakeslee, R. J., Bailey, J., Freitas, S.,
 - Lima, W. F. A., and Tokay, A.: The Chuva Project: How Does Convection Vary across Brazil?, Bulletin of the American Meteorological Society, 95, 1365–1380, https://doi.org/10.1175/bams-d-13-00084.1, 2014a.
 - Machado, L. A. T., Silva Dias, M. A. F., Morales, C., Fisch, G., Vila, D., Albrecht, R., Goodman, S. J., Calheiros, A. J. P., Biscaro, T., Kummerow, C., Cohen, J., Fitzjarrald, D., Nascimento, E. L., Sakamoto, M. S., Cunningham, C., Chaboureau, J.-P., Petersen, W. A.,
- Adams, D. K., Baldini, L., Angelis, C. F., Sapucci, L. F., Salio, P., Barbosa, H. M. J., Landulfo, E., Souza, R. A. F., Blakeslee, R. J., Bailey, J., Freitas, S., Lima, W. F. A., and Tokay, A.: The Chuva Project: How Does Convection Vary across Brazil?, Bulletin of the American Meteorological Society, 95, 1365–1380, https://doi.org/10.1175/BAMS-D-13-00084.1, 2014b.
 - Machado, L. A. T. T., Calheiros, A. J. P. P., Biscaro, T., Giangrande, S., Dias, M. A. F. S., Cecchini, M. A., Albrecht, R., Andreae, M. O., Araujo, W. F., Artaxo, P., Borrmann, S., Braga, R., Burleyson, C., Eichholz, C. W., Fan, J., Feng, Z., Fisch, G. F., Jensen, M. P., Martin,
- 370 S. T., Poschl, U., Pohlker, C., Pohlker, M. L., Ribaud, J.-F. F., Rosenfeld, D., Saraiva, J. M. B. B., Schumacher, C., Thalman, R., Walter, D., Wendisch, M., Dias, M. A. F. S., Cecchini, M. A., Albrecht, R., Andreae, M. O., Araujo, W. F., Artaxo, P., Borrmann, S., Braga, R., Burleyson, C., Eichholz, C. W., Fan, J., Feng, Z., Fisch, G. F., Jensen, M. P., Martin, S. T., Poschl, U., Pohlker, C., Pohlker, M. L., Ribaud,

- J.-F. F., Rosenfeld, D., Saraiva, J. M. B. B., Schumacher, C., Thalman, R., Walter, D., Wendisch, M., Dias, M. A. F. S., Cecchini, M. A., Albrecht, R., Andreae, M. O., Araujo, W. F., Artaxo, P., Borrmann, S., Braga, R., Burleyson, C., Eichholz, C. W., Fan, J., Feng, Z., Fisch,
 G. F., Jensen, M. P., Martin, S. T., Poschl, U., Pohlker, C., Pohlker, M. L., Ribaud, J.-F. F., Rosenfeld, D., Saraiva, J. M. B. B., Schumacher, C., Thalman, R., Walter, D., and Wendisch, M.: Overview: Precipitation characteristics and sensitivities to environmental conditions during GoAmazon2014/5 and ACRIDICON-CHUVA, Atmospheric Chemistry and Physics, 18, 6461–6482, https://doi.org/10.5194/acp-18-6461-2018, 2018.
- Makris, A. and Prieur, C.: Bayesian multiple-hypothesis tracking of merging and splitting targets, IEEE transactions on geoscience and remote sensing: a publication of the IEEE Geoscience and Remote Sensing Society, 52, 7684–7694, https://doi.org/10.1109/tgrs.2014.2316600, 2014.
 - Martin, S. T., Artaxo, P., Machado, L. A. T., Manzi, A. O., Souza, R. A. F., Schumacher, C., Wang, J., Andreae, M. O., Barbosa, H. M. J., Fan, J., Fisch, G., Goldstein, A. H., Guenther, A., Jimenez, J. L., Pöschl, U., Silva Dias, M. A., Smith, J. N., and Wendisch, M.: Introduction: Observations and Modeling of the Green Ocean Amazon (GoAmazon2014/5), Atmospheric Chemistry and Physics Discussions, 16, 30 175–30 210, https://doi.org/10.5194/acpd-15-30175-2015, 2016.

385

400

- Martin, S. T., Artaxo, P., Machado, L., Manzi, A. O., Souza, R. A. F., Schumacher, C., Wang, J., Biscaro, T., Brito, J., Calheiros, A., Jardine, K., Medeiros, A., Portela, B., de Sá, S. S., Adachi, K., Aiken, A. C., Albrecht, R., Alexander, L., Andreae, M. O., Barbosa, H. M. J., Buseck, P., Chand, D., Comstock, J. M., Day, D. A., Dubey, M., Fan, J., Fast, J., Fisch, G., Fortner, E., Giangrande, S., Gilles, M., Goldstein, A. H., Guenther, A., Hubbe, J., Jensen, M., Jimenez, J. L., Keutsch, F. N., Kim, S., Kuang, C., Laskin, A., McKinney, K.,
- Mei, F., Miller, M., Nascimento, R., Pauliquevis, T., Pekour, M., Peres, J., Petäjä, T., Pöhlker, C., Pöschl, U., Rizzo, L., Schmid, B., Shilling, J. E., Silva Dias, M. A., Smith, J. N., Tomlinson, J. M., Tóta, J., and Wendisch, M.: The Green Ocean Amazon Experiment (GoAmazon2014/5) Observes Pollution Affecting Gases, Aerosols, Clouds, and Rainfall over the Rain Forest, Bulletin of the American Meteorological Society, 98, 981–997, https://doi.org/10.1175/BAMS-D-15-00221.1, 2017.
- Murphy, M. J. and Nag, A.: Cloud lightning performance and climatology of the U.S. based on the upgraded U.S. National Lightning Detection Network, 2015.
 - Naccarato, K. P., Pinto, Jr, O., Garcia, S. A. M., Murphy, M., Demetriades, N., and Cramer, J.: Validation of the new GLD360 dataset in Brazil: First results, in: International Lightning Detection Conference, 2010.
 - Nobre, C. A., Obregón, G. O., Marengo, J. A., Fu, R., and Poveda, G.: Characteristics of Amazonian climate: Main features, in: Amazonia and Global Change, Geophysical monograph, pp. 149–162, American Geophysical Union, Washington, D. C., ISBN 9780875904764, https://agupubs.onlinelibrary.wiley.com/doi/abs/10.1029/2009GM000903, 2009.
 - Petersen, W. A. and Rutledge, S. A.: Regional Variability in Tropical Convection: Observations from TRMM, Journal of climate, 14, 3566–3586, https://doi.org/10.1175/1520-0442(2001)014<3566:RVITCO>2.0.CO;2, 2001.
 - Rickenbach, T. M., Ferreira, R. N., Halverson, J. B., Herdies, D. L., and Silva Dias, M. A. F.: Modulation of convection in the south-western Amazon basin by extratropical stationary fronts, Journal of Geophysical Research, D: Atmospheres, 107, LBA 7–1–LBA 7–13, https://doi.org/10.1029/2000JD000263, 2002.
 - Saraiva, I., Silva Dias, M. A. F., Morales, C. A. R., and Saraiva, J. M. B.: Regional Variability of Rain Clouds in the Amazon Basin as Seen by a Network of Weather Radars, Journal of Applied Meteorology and Climatology, 55, 2657–2675, https://doi.org/10.1175/JAMC-D-15-0183.1, 2016.

- Schumacher, C. and Funk, A.: GoAmazon2014/5 Three-dimensional Gridded S-band Reflectivity and Radial Velocity from the SIPAM

 410 Manaus S-band Radar, Tech. rep., Oak Ridge National Lab.(ORNL), Oak Ridge, TN (United States). Atmospheric ..., https://www.osti.
 gov/biblio/1459573, 2018.
 - Silva Dias, M. A. F. and Carvalho, L. M. V.: The South American Monsoon System, in: The Global Monsoon System, vol. 9 of *World Scientific Series on Asia-Pacific Weather and Climate*, pp. 25–33, World Scientific, ISBN 9789813200906, https://doi.org/10.1142/9789813200913_0003, 2016.
- Silva Dias, M. A. F., Rutledge, S., Kabat, P., Silva Dias, P. L., Nobre, C., Fisch, G., Dolman, A. J., Zipser, E., Garstang, M., Manzi, A. O., Fuentes, J. D., Rocha, H. R., Marengo, J., Plana-Fattori, A., Sá, L. D. A., Alvalá, R. C. S., Andreae, M. O., Artaxo, P., Gielow, R., and Gatti, L.: Cloud and rain processes in a biosphere-atmosphere interaction context in the Amazon Region, Journal of geophysical research, 107, S1, https://doi.org/10.1029/2001jd000335, 2002.
- Sokolowsky, G. A., Freeman, S. W., Jones, W. K., Kukulies, J., Senf, F., Marinescu, P. J., Heikenfeld, M., Brunner, K. N., Brunning, E. C.,
 Collis, S. M., Jackson, R. C., Leung, G. R., Pfeifer, N., Raut, B. A., Saleeby, S. M., Stier, P., and van den Heever, S. C.: *tobacv*1.5: introducing fast 3D tracking, splits and mergers, and other enhancements for identifying and analysing meteorological phenomena, Geoscientific model development, 17, 5309–5330, https://doi.org/10.5194/gmd-17-5309-2024, 2024.
 - Souza, C. M. A., Dias-Júnior, C. Q., D'Oliveira, F. A. F., Martins, H. S., Carneiro, R. G., Portela, B. T. T., and Fisch, G.: Long-term measurements of the Atmospheric Boundary Layer height in Central Amazonia using remote sensing instruments, Remote sensing, 15, 3261. https://doi.org/10.3390/rs15133261, 2023.

- Tian, Y., Zhang, Y., Klein, S. A., and Schumacher, C.: Interpreting the diurnal cycle of clouds and precipitation in the ARM GoAmazon observations: Shallow to deep convection transition, Journal of geophysical research, 126, https://doi.org/10.1029/2020jd033766, 2021.
- Uba, D. M., Negri, R. G., Enoré, D. P., Costa, I. C. d., and Jorge, A. A. S.: TATHU Software para rastreio e análise do ciclo de vida de sistemas convectivos, http://urlib.net/ibi/8JMKD3MGP3W34T/47AF772, 2022.
- Viscardi, L. A. M., Torri, G., Adams, D. K., and Barbosa, H. d. M. J.: Environmental controls on isolated convection during the Amazonian wet season, Atmospheric chemistry and physics, 24, 8529–8548, https://doi.org/10.5194/acp-24-8529-2024, 2024.
 - Yuter, S. E. and Houze, R. A.: Three-Dimensional Kinematic and Microphysical Evolution of Florida Cumulonimbus. Part II: Frequency Distributions of Vertical Velocity, Reflectivity, and Differential Reflectivity, Monthly Weather Review, 123, 1941–1963, https://doi.org/10.1175/1520-0493(1995)123<1941:tdkame>2.0.co;2, 1995.
- 435 Zhou, J. and Lau, K.-M.: Does a monsoon climate exist over South America?, Journal of climate, 11, 1020–1040, https://doi.org/10.1175/1520-0442(1998)011<1020:damceo>2.0.co;2, 1998.